HHS Public Access

Author manuscript

J Vis Exp. Author manuscript; available in PMC 2024 March 10.

A Protocol to Evaluate and Quantify Retinal Pigmented Epithelium Pathologies in Mouse Models of Age-Related Macular Degeneration

Michael Landowski[1,2], **Samuel Grindel**[1], **Ying Hao**[3], **Sakae Ikeda**[1,2], **Catherine Bowes Rickman**[3,4], **Akihiro Ikeda**[1,2]

[1]Department of Medical Genetics, University of Wisconsin-Madison

[2]McPherson Eye Research Institute, University of Wisconsin-Madison

[3]Department of Ophthalmology, Duke University

[4]Department of Cell Biology, Duke University

Abstract

Age-related macular degeneration (AMD) is a debilitating retinal disorder in aging populations. It is widely believed that dysfunction of the retinal pigmented epithelium (RPE) is a key pathobiological event in AMD. To understand the mechanisms that lead to RPE dysfunction, mouse models can be utilized by researchers. It has been established by previous studies that mice can develop RPE pathologies, some of which are observed in the eyes of individuals diagnosed with AMD. Here, we describe a phenotyping protocol to assess RPE pathologies in mice. This protocol includes the preparation and evaluation of retinal cross-sections using light microscopy and transmission electron microscopy, as well as that of RPE flat mounts by confocal microscopy. We detail the common types of murine RPE pathologies observed by these techniques and ways to quantify them through unbiased methods for statistical testing. As proof of concept, we use this RPE phenotyping protocol to quantify the RPE pathologies observed in mice overexpressing transmembrane protein 135 (*Tmem135*) and aged wild-type C57BL/6J mice. The main goal of this protocol is to present standard RPE phenotyping methods with unbiased quantitative assessments for scientists using mouse models of AMD.

Introduction

Age-related macular degeneration (AMD) is a common blinding disease that affects populations over the age of 55[1]. Many researchers believe that dysfunction within the retinal pigmented epithelium (RPE) is an early and crucial pathobiological event in AMD[2]. The RPE is a monolayer of polarized cells tasked with maintaining the homeostasis of neighboring photoreceptors and choroidal blood vessels[3]. A variety of models exist to

Corresponding Author Akihiro Ikeda, aikeda@wisc.edu.

A complete version of this article that includes the video component is available at http://dx.doi.org/10.3791/64927.

Disclosures

The authors of this protocol have no disclosures and conflicts of interest.

investigate disease-associated mechanisms within the RPE, including cell culture models[4,5] and mice[6,7,8]. A recent report has described standardized protocols and quality control criteria for RPE cell culture models[4], yet no report has attempted to standardize the phenotyping of the RPE in mouse models. In fact, many publications on mouse models of AMD lack a complete description of the RPE or quantification of the RPE pathologies in them. The overall goal of this protocol is to present standard RPE phenotyping methods with unbiased quantitative assessments for scientists using AMD mouse models.

Previous publications have noted the presence of several RPE pathologies in mice through three imaging techniques. For instance, light microscopy allows researchers to view the gross morphology of the murine retina (Figure 1A) and detect RPE pathologies such as RPE thinning, vacuolization, and migration. RPE thinning in an AMD mouse model is exemplified by a deviation in the RPE height from their respective controls (Figure 1B). RPE vacuolization can be divided into two separate categories: microvacuolization (Figure 1C) and macrovacuolization (Figure 1D). RPE microvacuolization is summarized by the presence of vacuoles in the RPE that do not affect its overall height, whereas macrovacuolization is indicated by the presence of vacuoles that protrude into the outer segments of the photoreceptors. RPE migration is distinguished by the focal aggregate of pigment above the RPE monolayer in a retinal cross-section (Figure 1E). It should be noted that migratory RPE cells in AMD donor eyes exhibit immunoreactivity to immune cell markers, such as cluster of differentiation 68 (CD68)[9], and could represent immune cells engulfing RPE debris or RPE undergoing transdifferentiation[9]. Another imaging technique called transmission electron microscopy can permit researchers to visualize the ultrastructure of the RPE and its basement membrane (Figure 2A). This technique can identify the predominant sub-RPE deposit in mice, known as the basal laminar deposit (BLamD) (Figure 2B)[10]. Lastly, confocal microscopy can reveal the structure of RPE cells through imaging RPE flat mounts (Figure 3A). This method can uncover RPE dysmorphia, the deviation of the RPE from its classic honeycomb shape (Figure 3B). It can also detect RPE multinucleation, the presence of three or more nuclei within an RPE cell (Figure 3C). For a summary of the types of RPE pathologies present in current AMD mouse models, we refer researchers to these reviews from the literature[6,7].

Researchers studying AMD should be aware of the advantages and disadvantages of using mice to investigate RPE pathologies prior to the phenotyping protocol. Mice are advantageous because of their relatively short life span and cost-effectiveness, as well as their genetic and pharmacologic manipulability. Mice also exhibit RPE degenerative changes, including RPE migration, dysmorphia, and multinucleation, that are observed in AMD donor eyes[11,12,13,14,15,16,17]; this suggests that similar mechanisms may underly the development of these RPE pathologies in mice and humans. However, there are key differences that limit the translatability of mouse studies to human AMD. First, mice do not have a macula, an anatomically distinct region of the human retina necessary for visual acuity that is preferentially affected in AMD. Second, some RPE pathologies in mice, like RPE thinning and vacuolization, are not typically seen in AMD donor eyes[18]. Third, mice do not develop drusen, a hallmark of AMD pathology[19]. Drusen are lipid- and protein-containing deposits with very few basement membrane proteins that form between the RPE basal lamina and the inner collagenous layer of Bruch’s membrane

(BrM)[19]. Drusen differ from BLamD, the common sub-RPE deposit in mice, in both their composition and anatomical location. BLamDs are age- and stress-dependent extracellular matrix-enriched abnormalities that form between the RPE basal lamina of BrM and the basal infoldings of the RPE[20]. Interestingly, BLamDs have a similar protein composition and appearance in both mice and humans[6,10,21]. Recent work suggests BLamDs may act in the pathobiology of AMD by influencing the progression of AMD to its later stages[18,22]; thus, these deposits may represent diseased RPE in the mouse retina. Knowledge of these benefits and limitations is critical for researchers interested in translating results from mouse studies to AMD.

In this protocol, we discuss the methods to prepare eyes for light, transmission electron, and confocal microscopy to visualize RPE pathologies. We also describe how to quantify RPE pathologies in an unbiased manner for statistical testing. As proof of concept, we utilize the RPE phenotyping protocol to investigate the structural RPE pathologies observed in transmembrane protein 135- (*Tmem135*) overexpressing mice and aged wild-type (WT) C57BL/6J mice. In summary, we aim to describe the phenotyping methodology to characterize the RPE in AMD mouse models, since there are currently no standard protocols available. Researchers interested in examining and quantifying pathologies of the photoreceptors or choroid, which are also affected in AMD mouse models, may not find this protocol useful for their studies.

Protocol

All procedures involving animal subjects have been approved by the Institutional Animal Care and Use Committee at the University of Wisconsin-Madison, and are in adherence with the Association for Research in Vision and Ophthalmology (ARVO) Statement for the Use of Animals in Ophthalmic and Vision Research.

1. Evaluation of mouse RPE by light microscopy

1. Make a fixative buffer that has a final concentration of 2% paraformaldehyde and 2% glutaraldehyde at room temperature (RT) in a glass bottle.

   NOTE: This protocol requires, at most, 14 mL of fixative buffer per mouse.

   CAUTION: Paraformaldehyde and glutaraldehyde are hazardous substances. Please follow the standard operating procedures when working with these substances.

2. Prepare a gravity-feed perfusion system on an absorbent underpad for cardiac perfusion in a fume hood (Supplementary Figure 1A).

   1. Place 40 mL of the fixative buffer into the syringe barrel of the perfusion system (Supplementary Figure 1B).

   2. Turn the valve until it is parallel with the tubing line to allow the buffer to flow through the tubing line (Supplementary Figure 1C). Flush the line with buffer until all air bubbles are removed from the line.

3. Turn the valve until it is perpendicular to the tubing line to stop the buffer from flowing into the tubing line (Supplementary Figure 1D).

   NOTE: The perfusion system is now ready for use.

3. Euthanize the mouse by placing it into a carbon dioxide (CO_2) chamber and allow CO_2 to flow into the chamber at a flow rate of 30% of the chamber volume per minute. Once the mouse stops breathing, allow CO_2 to flow into the chamber for at least 1 min. Verify the mouse is dead before moving forward to the next step.

   NOTE: Euthanasia through injection of pharmacological agents can be used in this protocol as an alternative to CO_2 inhalation.

4. Perform cardiac perfusion on the euthanized mouse.

   1. Transfer the mouse to a shallow tray near the perfusion system with its abdomen facing up. Spray the abdomen with 70% ethanol (EtOH).

   2. Make four incisions to expose the abdominal cavity (Supplementary Figure 2A).

      1. Create a 5 cm inferior cut using curved scissors and forceps through the skin and abdominal wall on the furthest left side of the mouse that is directly below the rib cage.

      2. Proceed to make a 3 cm medial cut through the skin and abdominal wall of the mouse that begins at the top of the inferior cut.

      3. Make another 5 cm inferior cut at the end of the medial cut through the skin and abdominal wall on the furthest right side of the mouse directly below the rib cage.

      4. Make another 3 cm medial incision to remove the abdominal skin flap with curved forceps.

   3. Cut through the diaphragm and sternum to expose the heart (Supplementary Figure 2B).

      NOTE: Be careful to avoid nicking the heart, arteries, and veins. Nicking these will lead to an inefficient cardiac perfusion.

   4. Insert the gauge needle into the left ventricle of the heart. Turn the valve until it is parallel with the tubing line. Cut the right atrium with curved scissors to allow blood and fixative to exit the heart (Supplementary Figure 2C).

   5. Allow 10 mL of fixative buffer to penetrate the mouse for at least 1–2 min, or until the liver becomes pale in color and no blood flows out of the right atrium. Once perfusion is complete, turn the valve until it is perpendicular to the tubing line to stop the flow of the buffer.

5. Enucleate the eyes from the mouse after cardiac perfusion.

1. Remove the mouse from the shallow tray and place the mouse on the absorbent underpad in a fume hood. Orient the head of the mouse such that the left eye is facing the experimenter and the right eye is out of view. Annotate the superior side of the eye with a tissue marking dye.

2. Gently push down with the thumb and index finger around the eye socket to cause protrusion of the eye from the eye socket (Supplementary Figure 3A).

3. Take curved scissors and hold it with the blade at a 30° angle from the eye socket. Proceed to cut around the eye with the curved scissors at a 30° angle (Supplementary Figure 3B).

   NOTE: It is okay to cut excess tissue from the eye socket to preserve the integrity of the eyeball.

4. Remove the eyeball from the head with curved forceps and place it on an absorbent underpad. Nick the cornea with a number 11 scalpel blade and place the eye with curved forceps into a 2 mL microtube with 2 mL of fixative buffer. Label the 2 mL microtube with mouse identification and 'left' to indicate the left eye.

   NOTE: The nick in the cornea allows for the fixative to readily penetrate the eye to better preserve it.

5. Repeat steps 1.5.1–1.5.4 for right eye.

6. Allow the eyes to incubate in fixative buffer overnight on a shaker in a 4 °Celsius (C) room, at a speed of 75 rotations per minute (rpm).

7. Replace the fixative buffer with 2 mL of 1x phosphate buffer saline (PBS). Incubate the eyes in 1x PBS for 10 min on a shaker at RT and 75 rpm. Repeat this step twice.

8. Clean and dissect the eyes to generate posterior segments.

   NOTE: The posterior segment is the mouse eyeball with the neural retina, RPE, choroid, and sclera sans the cornea, iris, and lens.

   1. Place eye into a Petri dish filled with 1x PBS under a dissecting microscope (Supplementary Figure 4A).

   2. Gently lift any fat and muscle away from the eyeball with fine-tipped forceps. Carefully trim the fat and muscle with micro-dissecting scissors in a parallel direction to the eyeball until the eyeball has a uniform bluish-black color (Supplementary Figure 4B).

      NOTE: Do not cut in a perpendicular direction, as this damages the eyeball. Also, if the tissue marking dye comes off during processing, reannotate the superior side of the eyeball immediately.

3. Place fine-tipped forceps at the corneal puncture site. Cut around the perimeter of the cornea, beginning at the puncture site, with micro-dissecting scissors, to remove the cornea and iris from the eyeball (Supplementary Figure 4C).

4. Take fine-tipped forceps and gently remove the lens from the eyeball to yield the posterior segment (Supplementary Figure 4D).

5. Place the posterior segment back into a 2 mL microtube with 2 mL of 1x PBS. Store the posterior segment in a 4 °C refrigerator.

   NOTE: Posterior segments can remain in 1x PBS at 4 °C for many weeks before further processing.

9. Repeat steps 1.3–1.8 to prepare the eyes from other mice in the study.

10. Process and embed one of the posterior segments from each mouse in paraffin for sectioning. Make sure the superior side of the posterior segment is on top.

    NOTE: The authors rely on the University of Wisconsin-Madison (UW) Translational Research Initiatives in Pathology (TRIP) laboratory to perform these tasks. Here are published protocols using a similar paraffin processing and embedding method[23,24].

11. Trim and section each paraffin block to obtain a 5 μm thick retinal section that includes the optic nerve head, as well as four additional 5 μm thick retinal sections that are 250 μm apart from each other. Label the slides with mouse identification and the serial section number (i.e., 1, 2, 3, 4, or 5). Store the slides in a slide box.

    NOTE: The authors rely on the UW TRIP laboratory for their services in paraffin sectioning. Here are published protocols using similar paraffin sectioning method[25,26].

12. Stain the slides containing retinal sections with hematoxylin and eosin (H&E). A protocol of H&E staining can be found in Supplementary Figure 5.

    NOTE: All steps of the H&E staining procedure must be completed in a fume hood.

13. Collect stitched images of H&E-stained retinal sections with a scale bar using a light microscope at 20x magnification.

14. Quantify the RPE thickness in the retinal images containing the optic nerve head for each sample.

    1. Download and open the Fiji ImageJ program. Drag all the stitched retinal images containing the optic nerve head into the

Fiji ImageJ taskbar. Verify the image scale is calibrated in μm and not pixels.

NOTE: The image scale is located in the upper lefthand corner of the window containing a retinal image in the Fiji ImageJ program. If the scale is set in pixels, please refer to the instruction manual of the Fiji ImageJ program to convert pixels to μm.

2. Mark every 300 μm interval in each image from the edge of the optic nerve head to the end of the retina (ora serrata). Click on the **Straight** icon in the Fiji ImageJ taskbar. Click and drag a line from the edge of the optic nerve head toward the ora serrata that is 300 μm in length. Click on the **Paintbrush** tool in the Fiji ImageJ taskbar and click the end of the 300 μm line to mark it.

3. Measure the RPE thickness at each marked interval. Click on the **Straight** icon in the Fiji ImageJ taskbar. Click and drag a line from the top to the bottom of the RPE (Supplementary Figure 6). Click on **Analyze > Measure** in the Fiji ImageJ menu bar to obtain the RPE thickness.

4. Transfer the RPE thickness measurements to a spreadsheet and label the column containing measurements with mouse identification. Label an additional column with 'Marked Interval' and enter the distance away from optic nerve values (i.e., 300, 600, 900, etc.)

   NOTE: The first measured interval corresponds to 300 μm away from the optic nerve, the second measured interval corresponds to 600 μm away, and so on.

15. Quantify RPE pathology incidence rates based on the retinal images for each sample.

    1. Open the Fiji ImageJ program.

    2. Open the **Cell Counter** application within the Fiji ImageJ program. Click on **Plugins > Analyze > Cell Counter** in the Fiji ImageJ menu bar. Drag a retinal image into the Fiji ImageJ taskbar and click on **Initialize** in the **Cell Counter** window.

    3. Count the number of RPE pathologies per retinal section using the **Cell Counter** application. Click on **Type 1** under **Counters** and then click on all microvacuolization events in the image. Click on **Type 2** under **Counters** and then click on all macrovacuolization events in the image. Click on **Type**

3 under **Counters** and then click on all individual migration events in the image.

4. Transfer the numbers of the RPE pathologies to a spreadsheet. Label the rows with either microvacuolization, macrovacuolization, or migration, and the column with mouse identification.

5. Repeat steps 1.15.2–1.15.4 for other images of the sample. Average the number of RPE pathologies per sample and divide by five to calculate the incidence rate of each RPE pathology for the sample in the spreadsheet.

16. Perform statistical analysis on the RPE thicknesses at each interval and the RPE pathology incidence rates to determine if there are significant differences between groups in the study.

2. Evaluation of mouse RPE by transmission electron microscopy

1. Cut the other posterior segments yielded after steps 1.5–1.9 in half through the superior mark into two sections with a razor blade. Reannotate the superior side of the sectioned posterior segments with tissue marking dye. Separate the sectioned posterior segments into new 2 mL microtubes containing 2 mL of 1x PBS and mouse identification.

   NOTE: The mouse posterior segment is too large to process in one piece and must be cut in half for transmission electron microscopy processing.

2. Rinse the tissues with 2 mL of 0.1 M cacodylate buffer, pH 7.2. Incubate for 10 min at RT on the benchtop. Repeat this step two more times.

3. Replace the 0.1 M cacodylate buffer with 2 mL of 2% osmium tetroxide (OsO_4) diluted in 0.1 M cacodylate buffer. Incubate for 1.5 h at RT in the fume hood.

   CAUTION: OsO_4 is a poisonous substance. Please follow standard operating procedures when working with OsO_4.

4. Rinse the tissues with 2 mL of 0.1 M cacodylate buffer for 10 min at RT in the fume hood. Repeat this step once.

5. Dehydrate the tissues with graduated EtOH dilutions ranging from 50% to 100% at RT in the fume hood. A protocol for the dehydration procedure can be found in Supplementary Figure 7.

6. Remove 100% EtOH from the tissues and add 2 mL of propylene oxide to tissues. Incubate at RT in the fume hood for 15 min. Remove the propylene oxide from the tissues and add 2 mL of fresh propylene oxide to the tissues. Incubate at RT in the fume hood for 15 min.

   CAUTION: Propylene oxide is a toxic substance. Please follow standard operating procedures when working with propylene oxide.

7. Remove propylene oxide from the tissues and add 2 mL of a 1:1 mixture of propylene oxide and resin to the tissues. Leave overnight under a vacuum in the fume hood at RT.

   CAUTION: Resin is a hazardous substance to humans. Please follow the laboratory's standard operating procedures when working with resin.

8. Replace the 1:1 mixture of propylene oxide and resin from tissues with 2 mL of pure resin. Leave overnight under a vacuum in the fume hood at RT.

9. Embed the tissues in resin. Place a label with mouse identification in pencil and a drop of resin into the mold . Position the tissue on the drop of resin. Fill the mold with resin and place under a vacuum for 1 h at RT in the fume hood.

10. Reposition the labels and specimens with fine-tipped forceps, with the posterior side of the posterior eyecup section on top. Leave the mold overnight at 65 °C in an oven in the fume hood.

11. Remove the molds from oven. Allow the molds to cool to RT on the benchtop. Remove the blocks from the molds.

    NOTE: The blocks are now ready for trimming.

12. Shape the resin blocks with a razor blade to form a trapezoid. Trim the resin blocks using a microtome until the optic nerve head is visible. Proceed to use a diamond knife to cut semithin sections from the resin blocks with a thickness of 0.5 μm.

    NOTE: Here is a published protocol on microtome sectioning[27]. If desired, 0.5 μm thick semithin sections from the resin blocks can be collected and stained to evaluate the integrity of the sample.

13. Cut a 70 nm thick ultrathin section from each trimmed block using an ultramicrotome. Collect a 70 nm thick ultrathin section on a 400-mesh thin-bar copper grid. Place the grid into a grid storage box and label the slot with mouse identification.

    NOTE: Here is a published protocol on ultramicrotome sectioning[28].

14. Stain the grids with 2% uranyl acetate for 5 min and then with 3.5% lead citrate solution for 5 min at RT in the fume hood.

    CAUTION: Uranyl acetate and lead citrate are hazardous substances. Please follow standard operating procedures when working with these substances.

15. Obtain images for each sample using a transmission electron microscope at a magnification of 15,000x, where the grid lines of the copper grid intersect the RPE and BrM.

    NOTE: There should be at least 20 to 35 images per section and 40 to 70 images per sample.

16. Quantify BLamD heights in the images for the samples in the study.

1. Open the Fiji ImageJ program. Drag all images from the sample section into the Fiji ImageJ taskbar. Verify that the images are calibrated in μm and not pixels.

2. Measure the BLamD height in the images. Click the Straight icon in the Fiji ImageJ taskbar. Click and drag a line from the elastic lamina of BrM to the top of the tallest deposit in the image (Supplementary Figure 8). Click **Analyze > Measure** in the Fiji ImageJ menu bar to obtain the BLamD height in the image.

   NOTE: If there are no BLamDs in the image, then draw a line from the elastic lamina of BrM to the basal lamina of the RPE.

3. Transfer the BLamD heights to a spreadsheet and label with mouse identification.

17. Calculate the cumulative frequencies of BLamD heights per genotype and averages of BLamD heights per mouse in the spreadsheet. Perform statistical analysis on the averages of BLamD heights to determine if there are significant differences between groups in the study.

3. Evaluation of mouse RPE through confocal microscopy

1. Collect eyes from the mice. Euthanize the mice according to the procedure described in step 1.3. Enucleate the eyes using step 1.5. Place the eyes using curved forceps into a 2 mL microtube with 2 mL of 1x PBS and mouse identification.

   NOTE: Do not dark-adapt the mice, as the interdigitization of the photoreceptors and RPE apical processes allows for better visualization of the RPE through confocal microscopy.

2. Clean and dissect the mouse eyes immediately to generate mouse posterior eyecups.

   NOTE: The posterior eyecup is different from the posterior segment because it does not contain the neural retina.

   1. Transfer the eye to a Petri dish containing 1x PBS under a dissecting microscope (Supplementary Figure 9A).

   2. Remove fat and muscle from the eyeball, as described in step 1.8.2 (Supplementary Figure 9B).

   3. Nick the cornea of the eyeball with a number 11 scalpel blade. Remove the cornea and iris, as detailed in step 1.8.3 (Supplementary Figure 9C).

   4. Pull out the lens with fine-tipped forceps. Take two fine-tipped forceps and gently separate the neural retina from the posterior segment.

   5. Carefully cut the neural retina at the optic nerve head for removal from the posterior eyecup (Supplementary Figure 9D).

6. Place the posterior eyecup into a new 2 mL microtube containing 500 µL of 1x PBS with mouse identification.

3. Fix the posterior eyecups with methanol (MeOH) (Supplementary Figure 10).

   NOTE: Step 3.3 takes about 2 h and 40 min to complete.

   1. Add 500 µL of MeOH to tissues. Incubate on a shaker at 75 rpm for 5 min at RT.
   2. Remove the 500 µL of solution from the tissues and add 500 µL of MeOH. Incubate for 5 min on a shaker at 75 rpm for 5 min at RT. Repeat this step one more time.
   3. Remove the entire solution from the tissues and add 500 µL of MeOH. Incubate on a shaker at 75 rpm for at least 2 h at RT.

      NOTE: As an alternative to step 3.3.3, the posterior eyecup can be incubated overnight in MeOH on a shaker at 75 rpm in a 4 °C room.
   4. Add 500 µL of 1x PBS to the tissues. Incubate on a shaker at 75 rpm for 5 min at RT.
   5. Remove the 500 µL of solution from the tissues and add 500 µL of 1x PBS. Incubate on a shaker at 75 rpm for 5 min at RT. Repeat this step one more time.
   6. Remove the entire solution from the tissues and replace it with 500 µL of 1x PBS.

      NOTE: The tissues are fully fixed by the MeOH and can be kept in a 4 °C refrigerator for at least 1 month.

4. Perform immunofluorescence staining of the posterior eyecups to visualize tight junctions and nuclei of the RPE (Supplementary Figure 11).

   1. Remove the 500 µL of 1x PBS from samples and add 100 µL of diluted 10% normal donkey serum in 1x PBS solution. Incubate on a shaker at 75 rpm for 30 min at RT.
   2. Remove the diluted 10% normal donkey serum solution from the samples and add 100 µL of a 1:50 dilution of a rabbit polyclonal anti-Zonula Occludens-1 (ZO-1) antibody in 1x PBS. Transfer the samples to a 4 °C room and incubate overnight on a shaker at 75 rpm.
   3. Remove the antibody dilution from the samples and add 2 mL of 1x PBS. Incubate on a shaker at 75 rpm for 10 min at RT. Repeat this step two more times.
   4. Remove the 1x PBS from samples. Add 100 µL of a 1:250 dilution of a donkey anti-rabbit IgG antibody with a 488 fluorophore-conjugated tag and a 1:250 dilution of 4’,6-Diamidine-2’-phenylindole dihydrochloride (DAPI) in 1x PBS to the samples. Cover the samples with aluminum foil and incubate on a shaker at 75 rpm for 2 h at RT.

NOTE: The samples must be completely covered with aluminum foil to prevent photobleaching.

5. Remove the antibody and DAPI dilutions from the samples. Add 2 mL of 1x PBS to the samples, recover with aluminum foil, and incubate on a shaker at 75 rpm for 10 min at RT. Repeat this step three more times.

   NOTE: The tight junctions and nuclei of the RPE are now fully labeled and stained, respectively.

5. Mount the posterior eyecups onto microscope slides.

   1. Label a microscope slide with mouse identification. Transfer the posterior eyecup onto a microscope slide under a dissecting microscope with the choroidal side facing down. Add a drop of 1x PBS to the posterior eyecup to prevent it from drying out (Supplementary Figure 12).

   2. Cut the posterior eyecup using a number 11 scalpel blade at four spots that will yield four quadrants corresponding to the cardinal directions (i.e., north, east, south, and west). Dab excess 1x PBS with the perimeter of the posterior eyecup. Gently flatten the posterior eyecup with a camel hairbrush and fine-tipped forceps (Supplementary Figure 12).

      NOTE: The resulting product is now known as an RPE flat mount.

   3. Add a drop of mounting medium to the RPE flat mount and place a coverslip on top of it. Apply clear fingernail polish to seal the coverslip and allow it to dry for at least 30 min at RT in a closed drawer. Place the slides in a slide carrier box and keep the box in a 4 °C refrigerator.

      NOTE: Be careful to avoid introducing bubbles on the RPE flat mount. RPE flat mounts can be imaged within a 2 week time frame.

6. Obtain an image of each of the four quadrants surrounding the optic nerve of the RPE flat mount on a confocal microscope at 20x magnification for each sample. An example of an RPE flat mount image can be found in Supplementary Figure 13A.

   NOTE: It may be necessary to perform z-stack imaging of the RPE flat mounts where multiple images are taken and stacked to compensate for dimensional differences of the RPE flat mount.

7. Trace the tight junctions of the RPE cells within each RPE flat mount image. An example of a traced RPE flat mount image can be found in Supplementary Figure 13B.

   1. Open the Fiji ImageJ program. Drag an RPE flat mount image into the Fiji ImageJ taskbar. Verify the image is calibrated in micrometers and not pixels.

2. Double-click on the **Overlay Brush Tool** icon in the Fiji ImageJ taskbar to set the brush width to 3, transparency to 0, and color to red. Click the **Close** button in the **Overlay Brush Tool** window.

3. Click on the **Overlay Brush Tool** icon. Click and drag on the tight junctions of all RPE cells that are completely within the image.

   NOTE: In case a tracing mistake is made, double-click on the **Overlay Brush Tool** icon and click the **Undo** box in the **Overlay Brush Tool** window to remove the tracing mistake from the image.

4. Click the **Rectangle** icon in the Fiji ImageJ taskbar. Click on the image and drag around the perimeter of the image. Click **Edit > Clear** on the Fiji ImageJ menu bar to keep the traced lines and remove any blue and green colors from the image.

5. Save the trace image in an appropriate location with mouse identification, quadrant location (i.e., north, south, east, or west), and a CP suffix label.

   NOTE: Do not save the RPE trace image prior to completing step 3.7.4.

8. Calculate the RPE cell areas for each sample.

   1. Designate a location to save the files from RPE area analysis by creating a folder on the computer desktop screen. Generate subfolders for each RPE trace image and label the subfolders with mouse identification as well as quadrant location (i.e., north, south, east, or west).

   2. Install and open the Cell Profiler program[29]. Download the Ikeda_RPE Area Calculator.cpproj (Supplementary Coding File 1) project file. Open the Ikeda_RPE Area Calculator.cpproj file by clicking **File > Open Project** in the Cell Profiler program menu bar.

   3. Drag one RPE trace image into **Image > Drop Files and Folders Here** box in the Cell Profiler program window.

   4. Input the location of the folder into the Cell Profiler program that corresponds to the RPE trace image. Click on the **Output Settings** button in the bottom left-hand corner of the Cell Profiler program window and enter the location of the folder in the **Default Input Folder** and **Default Output Folder** text boxes.

   5. Click on the **Analyze Images** button in the bottom left corner of the Cell Profiler program window. After the analysis is complete, an **Analysis Complete** window will appear on the screen. Click on the **OK** button in the **Analysis Complete** window.

      NOTE: This action will generate a csv file and jpeg image. The csv file will contain the areas for the RPE cells within the trace image. The jpeg

image will correspond to the RPE trace image, where each RPE cell will be labeled with a number (Supplementary Figure 13C).

6. Transfer the RPE areas from the csv file to a spreadsheet. Label the spreadsheet with mouse identification.

7. Perform a quality control survey of the data by confirming that each RPE area in the csv file links to a fully-traced RPE cell in a jpeg image. Remove any values from the spreadsheet that do not correspond to fully traced RPE cells.

8. Return to the Cell Profiler program. Right-click on the RPE trace image name in the **Drop Files and Folders Here** box and select **Clear the List** to remove the image from the Cell Profiler program.

9. Repeat steps 3.8.3–3.8.8 to calculate the RPE sizes for the remaining three RPE trace images of the sample.

9. Quantify the RPE cell size averages for each sample in the spreadsheet.

10. Quantify the RPE cell densities for each sample in the spreadsheet. To calculate the RPE cell density, divide the total number of RPE cells per quadrant by the total area of RPE cells per quadrant that was detected by the Cell Profiler program. Determine the average of the RPE cell densities from the four quadrants per sample.

11. Quantify the number of multinucleated RPE cells per RPE flat mount for each sample. Use the **Cell Counter** application within the Fiji ImageJ program, as described in steps 1.15.1–1.15.3, to count the number of RPE cells with more than three nuclei in four quadrants of the sample.

12. Perform statistical analysis on the RPE cell size and density averages, as well as the number of multinucleated RPE cells to determine if there are significant differences between groups in the study.

Representative Results

Completion of the RPE phenotyping protocol described in this article provides a quantitative analysis of the structural RPE abnormalities commonly observed in mouse models of AMD. To confirm the effectiveness of this protocol, we used it in mice that are known to display RPE pathologies, including transgenic mice that overexpress WT *Tmem135* driven by the chicken beta-actin promoter (*Tmem135* TG)[30] and aged C57BL/6J mice[31,32]. The objective of these experiments is to show representative results that could be obtained using the methods described in this protocol to researchers new to mouse models.

We adhered to the methods in **Step 1** of the protocol to process and evaluate eyes from WT and *Tmem135* TG mice to evaluate RPE pathologies using light microscopy. We found that 4-month-old *Tmem135* TG mice have a significant reduction in RPE thickness at two measured intervals relative to age-matched WT through an ANOVA with post-hoc Tukey

test (Figure 4). These results indicate that the RPE is thinner in the 4-month-old *Tmem135* TG mice than in age-matched WT mice at 600 and 900 μm away from the optic nerve.

In addition, utilizing the methods of **Step 1** of the protocol, we calculated the incidence of RPE pathologies, including microvacuolization, macrovacuolization, and migration of three 25-day-old WT and *Tmem135* TG mice (Figure 5A). The average frequency of RPE microvacuolization pathologies per slide in WT mice was 0.67 ± 0.31 and in *Tmem135* TG mice was 7.07 ± 0.61 (Figure 5B). There was no RPE macrovacuolization in WT mice, but there were, on average, 5.33 ± 2.02 macrovacuolization events in *Tmem135* TG mice (Figure 5C). Lastly, the rates of migratory RPE cells per slide was zero in WT mice and 0.4 ± 0.35 in *Tmem135* TG mice (Figure 5D). After performing a student's t-test, the incidence of RPE microvacuolization and microvacuolization was significantly different between WT and *Tmem135* TG mice. However, the higher incidence of RPE migratory cells in *Tmem135* TG mice was not significantly different compared to WT ($p = 0.1161$). This data shows that RPE microvacuolization and macrovacuolization, but not migration, is significantly higher in 25-day-old *Tmem135* TG than WT mice.

Following the methods of the protocol included in **Step 2**, we prepared retinal sections from 2-month-old and 24-month-old WT C57BL/6J mice for transmission electron microscopy to analyze the presence and heights of BLamDs. We found BLamDs present in 24-month-old WT retinas that were notably absent in 2-month-old WT retinas (Figure 6A). We presented the heights of the BLamDs in the 24-month-old WT retinas by calculating and plotting the cumulative frequencies of their occurrence. Cumulative frequencies of the BLamD heights were graphed against deposit height to illustrate the distribution of the deposit heights. There is a shift to the right of the line for the 24-month-old WT BLamD heights compared to the 2-month-old WT BLamD heights, demonstrating an increase of deposits in 24-month-old WT mice (Figure 6B). This graph is supported by a larger average of BLamD heights in 24-month-old WT retinas (1.01 μm ± 0.43 μm) than 2-month-old WT retinas (0.23 μm ± 0.017 μm), that were significantly different by a student's t-test (Figure 6C). In summary, we conclude that 24-month-old WT mice have large BLamDs in the sub-RPE space of their retinas compared to 2-month-old WT mice.

We applied the methods of preparing eyes from 4-month-old WT and *Tmem135* TG mice in **Step 3** to generate RPE flat mounts for the detection and analysis of RPE dysmorphia and multinucleation. In this protocol, we defined RPE dysmorphia by changes in RPE cell size and density in an AMD mouse model relative to their controls. We found that the RPE in 4-month-old *Tmem135* TG mice are dysmorphic (Figure 7A). The RPE in *Tmem135* TG retinas are larger (806.89 μm^2 ± 252.67 vs. 291.69 μm^2 ± 26.31) and less dense (0.0014 cells/μm^2 ± 0.00039 vs. 0.0033 cells/μm^2 ± 0.00024) than age-matched WT retinas (Figure 7B,C). Furthermore, there were more multinucleated RPE cells in the *Tmem135* TG retinas compared to WT controls (8.04 cells ± 5.54 vs. 0.33 cells ± 0.29) (Figure 7D). All these parameters reached statistical significance with a student's t-test. Together, 4-month-old *Tmem135* TG mice have more dysmorphic and multinucleated RPE cells than 4-month-old WT mice.

Discussion

In this article, we introduced a phenotyping protocol for assessing the structural RPE pathologies of mouse models. We described the steps required for processing the eyes for various imaging techniques including light, transmission electron, and confocal microscopy, as well as the quantitation of typical pathologies observed *via* these imaging methods. We proved the effectiveness of our RPE phenotyping protocol by examining *Tmem135* TG and 24-month-old WT mice, since these mice display RPE pathologies[30,31,32]. This protocol can be applied to any genetically modified or pharmacologically treated mouse that may harbor RPE pathologies such as RPE thinning, vacuolization, migration, and dysmorphia, as well as BLamDs[6,7]. Although the RPE pathologies observed in *Tmem135* TG and 24-month-old WT mice are present in other AMD mouse models[7,30], it is important for the researcher to become familiar with the AMD mouse model chosen for their studies, as the age of onset and severity of the RPE pathologies of their AMD mouse model may differ from the *Tmem135* TG and 24-month-old WT mice. Researchers may need to utilize more mice for their studies than the numbers of mice used to produce the representative results shown in this article, if the presentation of RPE pathologies is variable in their respective AMD mouse model. Furthermore, many AMD mouse models are currently available to AMD researchers, yet do not have complete descriptions of their RPE pathologies, which may require researchers to perform preliminary studies to acquire this information.

Although modifications can be made in how mouse eyes are processed for the various imaging methods, it is critical to maintain the quantitative evaluation of structural RPE abnormalities as described in the protocol. For instance, five H&E-stained retinal sections were prepared to count the number of RPE microvacuolization, macrovacuolization, and migration events, allowing researchers to evaluate RPE pathologies at multiple locations in the mouse retina. Another example is using a 400-mesh thin-bar copper electron microscopy grid to assess the ultrastructural abnormalities of the RPE. The electron microscopy grid provides a framework to evaluate a retinal sample systematically and unbiasedly by transmission electron micrography, as well as obtain 40 to 70 images per retinal section to examine the presence of BLamDs. This cannot be achieved with an electron microscopy-slot grid, and we suggest not utilizing them with this protocol. Lastly, capturing 20x magnification images from the four quadrants of an RPE flat mount enables researchers to investigate large areas of murine RPE for dysmorphia and multinucleation. Researchers are free to expand on this protocol and examine additional retinal sections for RPE pathologies in their studies. Together, these methods allow researchers to gather ample data to make conclusions about the structural RPE pathologies that may be present in their AMD mouse models.

Another key feature of this protocol is the consistency of the RPE phenotyping methods. For example, all eyes used for light and transmission electron microscopy were orientated by the superior side of the mouse retina for sectioning. It is important to maintain the orientation of the mouse eye throughout its processing for light and transmission electron microscopy because the mouse eye has a topographical distribution of retinal cells[33,34]. The anatomical orientation of the mouse eye was not maintained for RPE flat mount preparation, since superior to inferior topographical changes of the mouse RPE cell have not been observed.

In fact, the RPE in the human retina displays topographical changes that radiate away from the optic nerve head[35], suggesting this may be the case for mouse RPE. Lastly, the image acquisition described in this protocol relies on the anatomical positioning of the optic nerve. Inclusion of these methodological aspects will help to reproduce results of RPE pathologies for researchers as they work with their AMD mouse models.

Researchers may desire to add more analytical features to the RPE phenotyping protocol. Some phenotypic outcomes not featured in this protocol are the examination of BrM thickness, RPE apical microvilli, and other RPE ultrastructural components. These components include mitochondria, pigment granules, and other organelles like phagosomes. Researchers can determine the size and number of these components in the electron micrographs obtained with this protocol using the Fiji ImageJ program. In particular, the status of mitochondria may be an important phenotypic outcome to consider, since targeting mitochondria in the RPE is an important therapeutic strategy for AMD[36]. Another phenotypic outcome is additional measurements of RPE dysmorphia on RPE flat mounts. RPE flat mount images obtained using the protocol can be examined for RPE hexagonal shape, number of neighboring RPE cells, and other properties with the REShAPE program (https://github.com/nih-nei/REShAPE)[35]. Another possible phenotypic outcome is whether RPE pathologies occur in the central or peripheral areas of the mouse retina. These additional phenotypic considerations will further strengthen the RPE phenotyping protocol described in this article.

There are a few limitations of this RPE phenotyping protocol. One limitation of this method is the need to sacrifice mice to harvest their eyes for RPE phenotyping. As an alternative, new advances in spectral domain optical coherence tomography (SD-OCT) imaging allow for the quantification of RPE thickness and pathologies in living mice[37–39]. This may be advantageous to researchers who want to perform longitudinal studies on their AMD mouse model cohorts. Another limitation of this method is the lack of functional RPE assessments in mice. If researchers are interested in a functional assessment of the RPE in mice, we recommend performing electroretinography and measuring the c-wave component, as the c-wave is indicative of the functional role of the RPE in phototransduction[40]. Another limitation of this method is the lack of biochemical measurements of RPE markers in mice. If researchers desire to investigate the levels of RPE markers, such as cellular retinaldehyde-binding protein (CRABLP), retinal pigment epithelium-specific 65 kDa protein (RPE65), potassium inwardly rectifying channel subfamily J member 13 (KCNJ13), or bestrophin 1 (BEST1), we recommend harvesting eyes for immunohistochemistry, quantitative real-time PCR, or western blot analysis.

In conclusion, this RPE phenotyping protocol can be an important resource for researchers using mouse models recapitulating pathological aspects of AMD. This protocol also serves to standardize how the RPE is evaluated in AMD mouse models, which has not been previously described in the literature. Standardizing RPE phenotyping would be critical in translating the findings from mice to other models of AMD, including RPE cell culture models[4] and higher organism models including non-human primates. It would also aid in our understanding of the pathobiological mechanisms underlying AMD development and potentially developing new therapies for this blinding disease.

Supplementary Material

Refer to Web version on PubMed Central for supplementary material.

Acknowledgments

The authors would like to acknowledge Satoshi Kinoshita and the University of Wisconsin (UW) Translational Research Initiatives in Pathology laboratory (TRIP) for preparing our tissues for light microscopy. This core is supported by the UW Department of Pathology and Laboratory Medicine, University of Wisconsin Carbone Cancer Center (P30 CA014520), and the Office of The Director-NIH (S10OD023526). Confocal microscopy was performed at the UW Biochemistry Optical Core, which was established with support from the UW Department of Biochemistry Endowment. This work was also supported by grants from the National Eye Institute (R01EY022086 to A. Ikeda; R01EY031748 to C. Bowes Rickman; P30EY016665 to the Department of Ophthalmology and Visual Sciences at the UW; P30EY005722 to the Duke Eye Center;NIH T32EY027721 to M. Landowski; F32EY032766 to M. Landowski), Timothy William Trout Chairmanship (A. Ikeda), FFB Free Family AMD Award (C. Bowes Rickman); and an unrestricted grant from the Research to Prevent Blindness (Duke Eye Center).

References

1. Wong WL et al. Global prevalence of age-related macular degeneration and disease burden projection for 2020 and 2040: a systematic review and meta-analysis. The Lancet. Global Health. 2 (2), e106–116 (2014). [PubMed: 25104651]
2. Bhutto I, Lutty G Understanding age-related macular degeneration (AMD): relationships between the photoreceptor/retinal pigment epithelium/Bruch's membrane/choriocapillaris complex. Molecular Aspects of Medicine. 33 (4), 295–317 (2012). [PubMed: 22542780]
3. Lakkaraju A et al. The cell biology of the retinal pigment epithelium. Progess in Retinal and Eye Research. 100846 (2020).
4. Bharti K et al. Cell culture models to study retinal pigment epithelium-related pathogenesis in age-related macular degeneration. Experimental Eye Research. 222, 109170 (2022). [PubMed: 35835183]
5. Forest DL, Johnson LV, Clegg DO Cellular models and therapies for age-related macular degeneration. Disease Models & Mechanisms. 8 (5), 421–427 (2015). [PubMed: 26035859]
6. Landowski M, Bowes Rickman C Targeting lipid metabolism for the treatment of age-related macular degeneration: Insights from preclinical mouse models. Journal of Ocular Pharmacology and Therapeutics. 38 (1), 3–32 (2022). [PubMed: 34788573]
7. Pennesi ME, Neuringer M, Courtney RJ Animal models of age related macular degeneration. Molecular Aspects of Medicine. 33 (4), 487–509 (2012). [PubMed: 22705444]
8. Malek G, Busik J, Grant MB, Choudhary M Models of retinal diseases and their applicability in drug discovery. Expert Opinion on Drug Discovery. 13 (4), 359–377 (2018). [PubMed: 29382242]
9. Cao D et al. Hyperreflective foci, optical coherence tomography progression indicators in age-related macular degeneration, include transdifferentiated retinal pigment epithelium. Investigative Ophthalmology & Visual Sciences. 62 (10), 34 (2021).
10. Ding JD et al. Expression of human complement factor H prevents age-related macular degeneration-like retina damage and kidney abnormalities in aged Cfh knockout mice. The American Journal of Pathology. 185 (1), 29–42 (2015). [PubMed: 25447048]
11. Zanzottera EC et al. The project MACULA retinal pigment epithelium grading system for histology and optical coherence tomography in age-related macular degeneration. Investigative Ophthalmology & Visual Sciences. 56 (5), 3253–3268 (2015).
12. Ding JD et al. Anti-amyloid therapy protects against retinal pigmented epithelium damage and vision loss in a model of age-related macular degeneration. Proceedings of the National Academy of Sciences. 108 (28), E279–E287 (2011).
13. Zhang Q et al. Comparison of histologic findings in age-related macular degeneration with RPE flatmount images. Molecular Vision. 25, 70–78 (2019). [PubMed: 30820143]

14. von der Emde L et al. Histologic cell shape descriptors for the retinal pigment epithelium in age-related macular degeneration: A comparison to unaffected eyes. Translational Vision Science & Technology. 11 (8), 19 (2022).
15. Gambril JA et al. Quantifying retinal pigment epithelium dysmorphia and loss of histologic autofluorescence in age-related macular degeneration. Investigative Ophthalmology & Visual Sciences. 60 (7), 2481–2493 (2019).
16. Bird AC, Phillips RL, Hageman GS Geographic atrophy: a histopathological assessment. JAMA Ophthalmology. 132 (3), 338–345 (2014). [PubMed: 24626824]
17. Zanzottera EC et al. Visualizing retinal pigment epithelium phenotypes in the transition to geographic atrophy in age-related macular degeneration. Retina. 36 (Suppl 1), S12–S25 (2016). [PubMed: 28005660]
18. Sura AA et al. Measuring the contributions of basal laminar deposit and Bruch's membrane in age-related macular degeneration. Investigative Ophthalmology & Visual Sciences. 61 (13), 19 (2020).
19. Curcio CA Soft drusen in age-related macular degeneration: biology and targeting via the oil spill strategies. Investigative Ophthalmology & Visual Sciences. 59 (4), AMD160–AMD181 (2018).
20. Johnson M et al. Comparison of morphology of human macular and peripheral Bruch's membrane in older eyes. Current Eye Research. 32 (9), 791–799 (2007). [PubMed: 17882712]
21. Sarks SH, Arnold JJ, Killingsworth MC, Sarks JP Early drusen formation in the normal and aging eye and their relation to age related maculopathy: a clinicopathological study. The British Journal of Ophthalmology. 83 (3), 358–368 (1999). [PubMed: 10365048]
22. Chen L, Messinger JD, Kar D, Duncan JL,Curcio CA Biometrics, impact, and significance of basal linear deposit and subretinal drusenoid deposit in age-related macular degeneration. Investigative Ophthalmology & Visual Sciences. 62 (1), 33 (2021).
23. Canene-Adams K Preparation of formalin-fixed paraffin-embedded tissue for immunohistochemistry. Methods in Enzymology. 533, 225–233 (2013). [PubMed: 24182927]
24. Fischer AH, Jacobson KA, Rose J, Zeller R Paraffin embedding tissue samples for sectioning. CSH Protocols. 2008, pdb.prot4989 (2008).
25. Cornell WC et al. Paraffin embedding and thin sectioning of microbial colony biofilms for microscopic analysis. Journal of Visualized Experiments. (133), 57196 (2018). [PubMed: 29630036]
26. Qin C et al. The cutting and floating method for paraffin-embedded tissue for sectioning. Journal of Visualized Experiments. (139), 58288 (2018). [PubMed: 30247474]
27. Baena V, Schalek RL, Lichtman JW,Terasaki M Serial-section electron microscopy using automated tape-collecting ultramicrotome (ATUM). Methods in Cell Biology. 152, 41–67 (2019). [PubMed: 31326026]
28. Yamaguchi M, Chibana H A method for obtaining serial ultrathin sections of microorganisms in transmission electron microscopy. Journal of Visualized Experiments. (131), 56235 (2018). [PubMed: 29364224]
29. Stirling DR et al. CellProfiler 4: improvements in speed, utility and usability. BMC Bioinformatics. 22 (1), 433 (2021). [PubMed: 34507520]
30. Landowski M et al. Modulation of Tmem135 leads to retinal pigmented epithelium pathologies in mice. Investigative Ophthalmology & Visual Sciences. 61 (12), 16 (2020).
31. Mori H et al. Developmental and age-related changes to the elastic lamina of Bruch's membrane in mice. Graefe's Archive for Clinical and Experimental Ophthalmology. 257 (2), 289–301 (2019).
32. Chen M et al. Retinal pigment epithelial cell multinucleation in the aging eye - a mechanism to repair damage and maintain homoeostasis. Aging Cell. 15 (3), 436–445 (2016). [PubMed: 26875723]
33. Ortín-Martínez A et al. Number and distribution of mouse retinal cone photoreceptors: differences between an albino (Swiss) and a pigmented (C57/BL6) strain. PLoS One. 9 (7), e102392 (2014). [PubMed: 25029531]
34. El-Danaf RN, Huberman AD Sub-topographic maps for regionally enhanced analysis of visual space in the mouse retina. The Journal of Comparative Neurology. 527 (1), 259–269 (2019). [PubMed: 29675855]

35. Ortolan D et al. Single-cell-resolution map of human retinal pigment epithelium helps discover subpopulations with differential disease sensitivity. Proceedings of the National Academy of Sciences. 119 (19), e2117553119 (2022).

36. Brown EE, Lewin AS, Ash JD Mitochondria: Potential targets for protection in age-related macular degeneration. Advances in Experimental Medicine and Biology. 1074, 11–17 (2018). [PubMed: 29721922]

37. Puk O, De Angelis MH, Graw J Longitudinal fundus and retinal studies with SD-OCT: a comparison of five mouse inbred strains. Mammalian Genome. 24 (5–6), 198–205 (2013). [PubMed: 23681115]

38. Knott EJ, Sheets KG, Zhou Y, Gordon WC, Bazan NG Spatial correlation of mouse photoreceptor-RPE thickness between SD-OCT and histology. Experimental Eye Research. 92 (2), 155–160 (2011). [PubMed: 21035444]

39. Allen RS, Bales K, Feola A, Pardue MT In vivo structural assessments of ocular disease in rodent models using optical coherence tomography. Journal of Visualized Experiments. (161), 61588 (2020).

40. Wu J, Peachey NS, Marmorstein AD Light-evoked responses of the mouse retinal pigment epithelium. Journal of Neurophysiology. 91 (3), 1134–1142 (2004). [PubMed: 14614107]

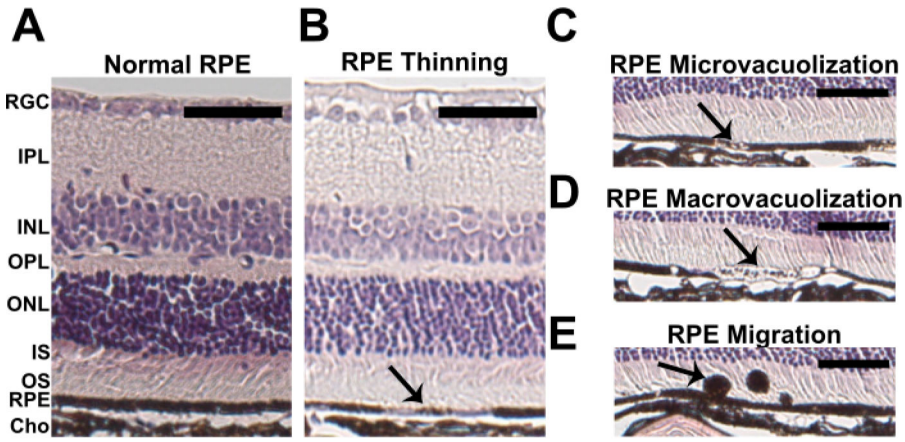

Figure 1: RPE pathologies detected by light microscopy.

Representative images of normal RPE in WT (**A**) and abnormal RPE in *Tmem135* TG mice (**B-E**). The RPE pathologies observed in *Tmem135* TG mice include RPE thinning (**B**), macrovacuolization (**C**), microvacuolization (**D**), and migration (**E**). Each pathology is illustrated by a black arrow. Scale bar = 100 μm. Magnification = 20x. Abbreviations: RGC = retinal ganglion cell layer, IPL = inner plexiform layer, INL = inner nuclear layer, OPL = outer plexiform layer, ONL = outer nuclear layer, IS = photoreceptor inner segments, OS = photoreceptor outer segments, RPE = retinal pigmented epithelium, Cho = choroid. Please click here to view a larger version of this figure.

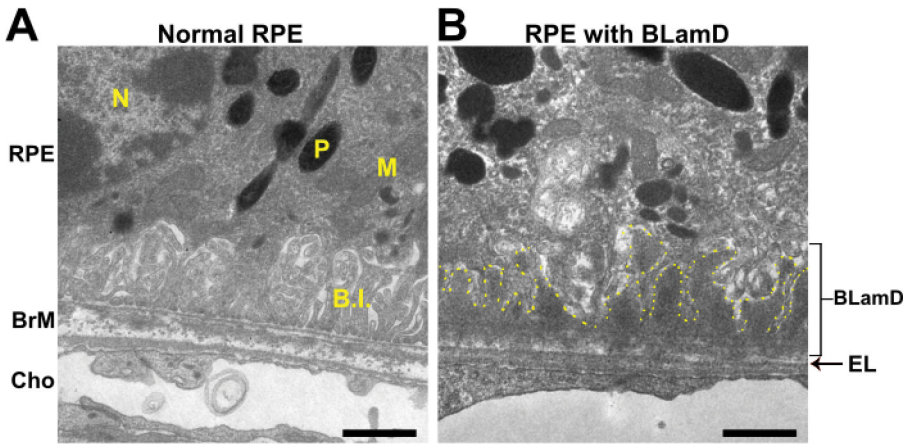

Figure 2: RPE pathologies detected by transmission electron microscopy.

Representative images of (**A**) RPE in young *CFH-H/H* and (**B**) 2-year-old *CFH-H/H* mice that has abundant basal laminar deposits (BLamDs). BLamDs are traced with yellow dots in the image. Scale bar = 800 nm. Magnification = 15,000x. Abbreviations: N = nucleus, M = mitochondrion, P = pigment granule, BI = basal infoldings, EL = elastic lamina, RPE = retinal pigmented epithelium, BrM = Bruch's membrane, Cho = choroid. Please click here to view a larger version of this figure.

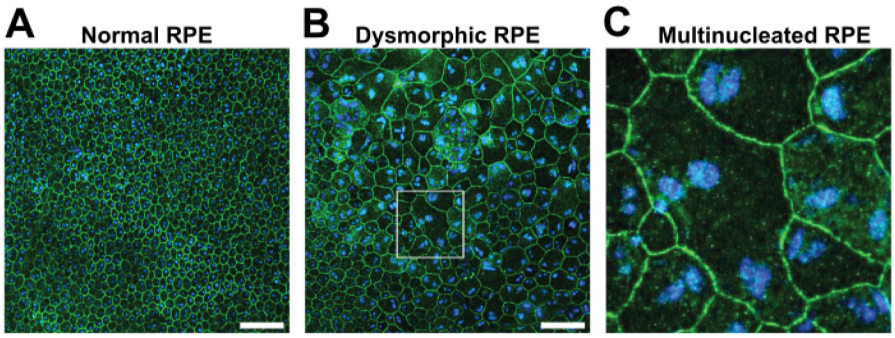

Figure 3: RPE pathologies detected by confocal microscopy.

Representative images of (**A**) normal RPE of 8-month-old WT and (**B**) abnormal RPE of 8-month-old *Tmem135* TG mice that exhibits RPE dysmorphia. The white square is zoomed in (**C**) to depict a multinucleated RPE cell with three nuclei. The green color is anti-ZO1 associated RPE tight junctions, and the blue color is DAPI staining of RPE nuclei. Scale bar = 50 μm. Magnification = 20x. Please click here to view a larger version of this figure.

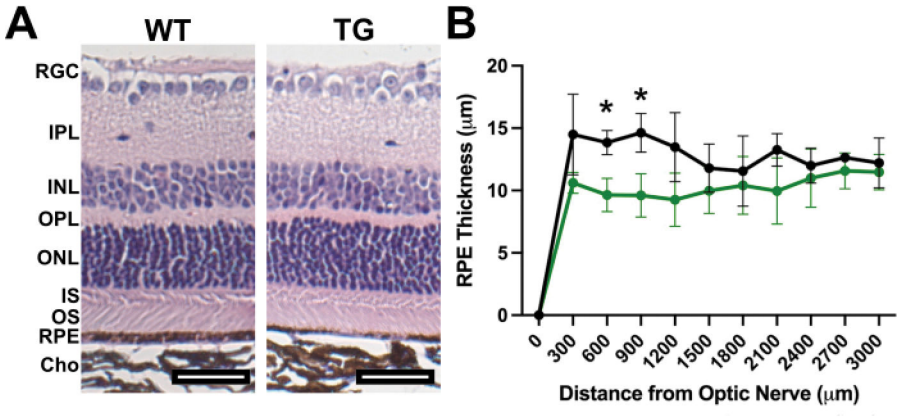

Figure 4: RPE thickness in 4-month-old wild-type (WT) and *Tmem135* TG mice.

(**A**) Representative images of the retina from 4-month-old WT and *Tmem135* TG (TG) mice. Magnification = 20x. Scale bar = 100 μm. (**B**) Line graphs of the RPE thickness measurements in 4-month-old WT (black) and *Tmem135* TG mice (green) up to 3,000 μm away from the optic nerve. Numbers after the genotype denote the number of mice used in this study. *$p < 0.05$, ANOVA with post-hoc Tukey test. All data are mean ± sd. Please see the Figure 1 legend for abbreviations of retinal layers. Please click here to view a larger version of this figure.

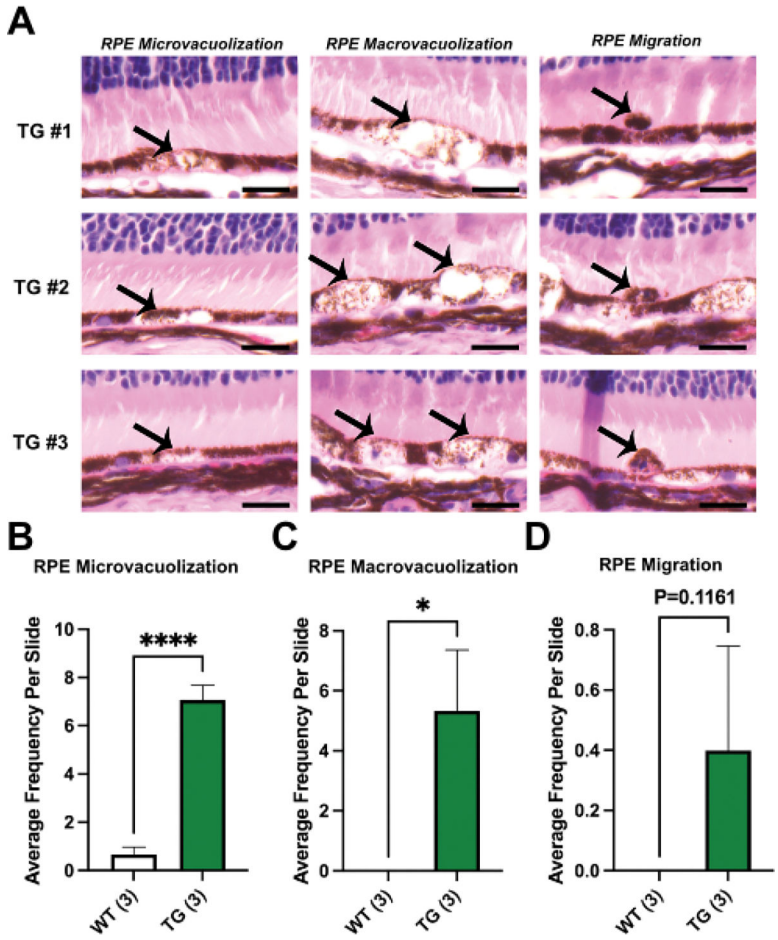

Figure 5: RPE pathologies in 25-day-old *Tmem135* TG mice.

(**A**) Representative images of RPE microvacuolization, macrovacuolization, and migration in three 25-day-old *Tmem135* TG (TG) mice. RPE pathologies are highlighted by black arrows in each image. Magnification = 40x. Scale bar = 20 μm. (**B-D**) Quantification of RPE micro- and macrovacuolization as well as migratory RPE cells in 25-day-old WT and *Tmem135* TG mice. Numbers in parentheses denote the number of mice used in this study. *$p < 0.05$ and ****$p < 0.0001$, student's t-test. All data are mean ± sd. Please click here to view a larger version of this figure.

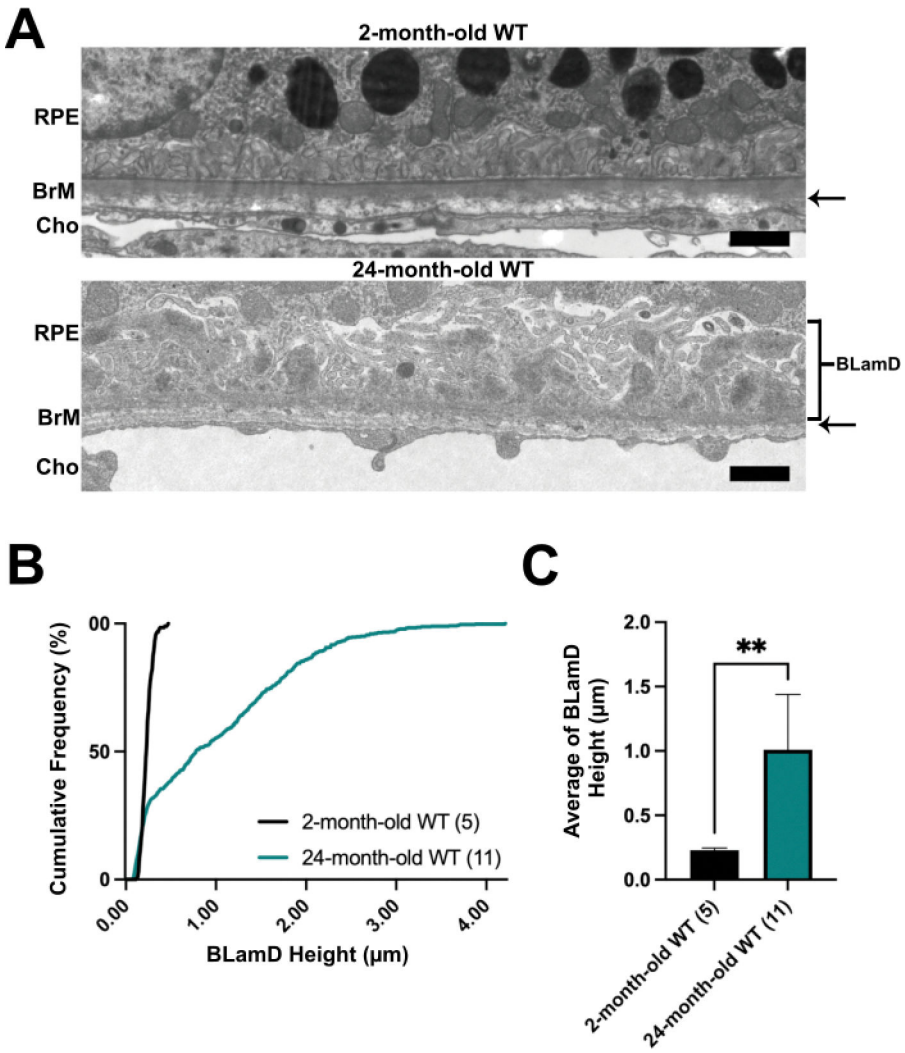

Figure 6: Ultrastructural analysis of BLamDs in young and aged WT retinas.

(**A**) Representative electron micrographs of 2-month-old and 24-month-old WT RPE. Magnification = 15,000x. Scale bar = 800 nm. An example of a basal laminar deposit (BLamD) is diagrammed with a bracket. (**B**) Cumulative frequencies of the BLamD heights. (**C**) BLamD height averages. Numbers in parentheses denote the total number of mice per genotype used in this study. $^{**}p < 0.01$, student's t-test. All data are mean ± sd. Please see the Figure 2 legend for abbreviations of retinal layers. Please click here to view a larger version of this figure.

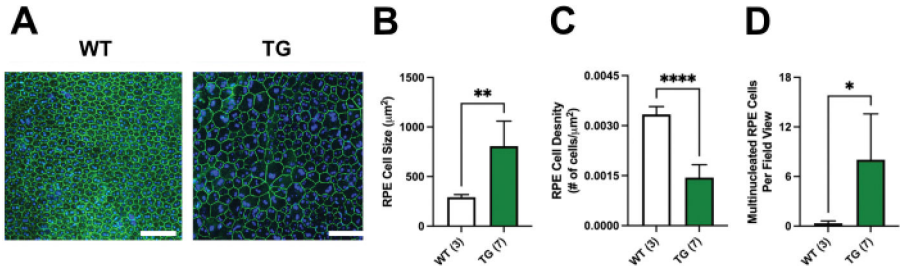

Figure 7: RPE flat mounts reveal RPE pathologies in *Tmem135* TG mice.

(**A**) Representative images of 4-month-old WT and *Tmem135* TG (TG) RPE flat mounts with anti-ZO-1 in green and DAPI in blue. Magnification = 20x. Scale bar = 100 μm. (**B**) RPE cell size, (**C**) RPE cell density, and (**D**) RPE multinucleation in 4-month-old WT and *Tmem135* TG mice. The number in parentheses denotes the number of mice used in the study. *$p < 0.05$, **$p < 0.01$ and ****$p < 0.0001$, student's t-test. All data are mean ± sd. Please click here to view a larger version of this figure.